Supplementary Information

Cage-Confinement Pyrolysis Route to Ultrasmall Tungsten Carbide Nanoparticles for Efficient Electrocatalytic Hydrogen Evolution

Yan-Tong Xu[a], Xiaofen Xiao[c], Zi-Ming Ye[a], Shenlong Zhao[d], Rongan Shen[b], Chun-Ting He*[a], Jie-Peng Zhang*[a], Yadong Li*[b], and Xiao-Ming Chen[a]

[a]*MOE Key Laboratory of Bioinorganic and Synthetic Chemistry, School of Chemistry, Sun Yat-Sen University, Guangzhou 510275, China*

[b]*Department of Chemistry, Tsinghua University, Beijing 100084, China*

[c]*Key Laboratory for Polymeric Composite and Functional Materials of Ministry of Education, Key Laboratory of High Performance Polymer-Based Composites of Guangdong Province, School of Chemistry, Sun Yat-Sen University, Guangzhou 510275, China.*

[d]*CAS Key Laboratory of Nanosystem and Hierarchical Fabrication, CAS Center for Excellence in Nanoscience, National Center for Nanoscience and Technology, Beijing 100190, China*

Email: hechunt@mail2.sysu.edu.cn; zhangjp7@mail.sysu.edu.cn; ydli@mail.tsinghua.edu.cn

S1. Experimental Section

All reagents were analytical grade and used without further purification. All solutions used in electrochemical experiments were prepared with Millipore water (≥ 18 MΩ).

Synthesis of MAF-6

MAF-6 was prepared following our published procedure.[1] Aqueous ammonia solution (40 mL 25%) of $Zn(OH)_2$ (2 mmol) was added into methanol solution (30 mL) of 2-ethylimidazole (4 mmol) premixed with cyclohexane (8 mL). The mixture was stirred vigorously at room temperature for several hours. The resultant white powders were separated from solution by filtration and then dried at 150 °C under vacuum for 2 hours.

Synthesis of $W(CO)_6$@MAF-6

MAF-6 (0.40 g) was placed in a 5-mL glass vial. This vial was placed in a glass bottle containing $W(CO)_6$ (0.66 mmol). The bottle was sealed and then heated under 85 °C for 24 hours. We also tried to reduce the amount of $W(CO)_6$ loading (0.275 mmol/g, or 9.1 wt%) to attain smaller WC particles, but the resultant sample showed similar WC particle sizes but less WC amount (Figure S11), as well as lower HER activity (Figure S19), as compared with titled material WC@NPC.

Synthesis of $W(CO)_6$/MAF-6

Aqueous ammonia solution (40 mL 25%) of $Zn(OH)_2$ (2 mmol) was dropped into a methanol solution (30 mL), which was premixed with 2-ethylimidazole (4 mmol), $W(CO)_6$ (0.4 mmol) and cyclohexane (8 mL). The mixture was stirred violently at room temperature for several hours. The resultant white powders were separated from solution by filtration and then dried at room temperature in air for 10 hours.

Synthesis of WC@NPC

$W(CO)_6$@MAF-6 (0.40 g) was carbonized under N_2 atmosphere in a tube furnace, where the temperature was raised up from 30 °C to 980 °C at a heating rate of 2.5 °C/min. After holding at

980 °C for 5 hours, the temperature was cooled down to room temperature naturally to afford black powder. For comparison, $W(CO)_6$@MAF-6 was also carbonized at three different temperatures (800, 900 and 1100 ^oC), but the lower temperatures are disadvantageous for the formation of WC (only W formation at 800^oC while mixing phases of WC and W formation at 900 ^oC as judged by PXRD measurements, Figure S5) and the vaporization of Zn (judging by the EDS measurements as shown in Table S2) while higher temperature resulted in collapsing of carbon nanopolyhedron (Figures S5 and S6). Also, the sample carbonized at 980^oC exhibits the best HER performances (Figure S18). Such worse performance of the samples carbonized at other temperatures should be resulted from the existence of lower active W and some residual inactive zinc (800 ^oC and 900 ^oC samples) or aggregation/non-uniform distribution on the surface of electrode for 1100 ^oC sample (collapsed/sintered carbon matrix was bad for affording homogenous catalyst ink by sonication). Therefore, WC@NPC used in this work refers to the sample carbonized at 980 ^oC.

Synthesis of W@NPC

$W(CO)_6$/MAF-6 (0.40 g) was carbonized under N_2 atmosphere in a tube furnace, where the temperature was raised up from 30 °C to 980 °C at a heating rate of 2.5 °C/min. After holding at 980 °C for 5 hours, the temperature was cooled down to room temperature naturally to afford black powder.

Characterizations

Powder X-Ray diffraction (PXRD) patterns were recorded on a D8 DAVANCI X-ray powder diffractometer equipped with graphite monochromatized Cu Kα radiation (λ = 1.5418 Å). The diffractometer was operated with working voltage and current of 40 kV and 40 mA, respectively. Transmission electron microscopy (TEM) and high-resolution TEM (HRTEM) images were recorded on a JEM-2010HR apparatus working at an accelerating voltage of 200 kV. Energy-dispersive X-ray spectroscopy (EDS) was taken on a JEM-2010HR-Vantage typed energy spectrometer. Particle size distribution (PSD) plots were measured manually through the nanoparticle statistical software (Image J) from corresponding TEM images with at least 80 particles. Field-emission scanning electron microscopy (FE-SEM) was carried out with a Hitachi SU8010 apparatus working at an

acceleration voltage of 2 kV. X-ray photon spectroscopy (XPS) was performed on an ESCA Lab250 X-ray microprobe corrected by C1s peak at 284.6 eV. Nitrogen sorption experiments were operated at 77 K on a Micromeritics ASAP 2020 system. Prior to the measurement, the samples were degassed at 120°C for 10 h. Thermogravimetry (TG) was performed on a TA Q50 system under N_2 flow. Fourier transformed-infrared (FT-IR) spectra were recorded on a Bruker TENSOR 27 FT-IR spectrometer in the 400–4000 cm^{-1} region with KBr pellets. Raman spectra were recorded by a Nicolet NXR 9650 FT-Raman Spectrometer.

Electrochemical Measurements

All electrochemical experiments were conducted on a CHI 660 E electrochemical station (Shanghai Chenhua Co., China) in a standard three electrode cell in N_2-saturated 0.5 M H_2SO_4 at room temperature. A glassy carbon electrode (GCE, 5 mm in diameter), an Ag/AgCl electrode with saturated KCl, and a Pt wire were used as the working, reference and counter electrode, respectively. The possibility of Pt-deposition of the working electrode for HER electrocatalysis was excluded by the virtually identical LSV curves of WC@NPC by using Pt and graphite as counter electrodes (Figure S20), similar XPS results before and after HER testing (Figure S23), and almost no change of the current density during long-term electrolysis by using either a Pt or a graphite counter electrode (Figure S20b). Besides, the LSV curve of WC@NPC with H_2 bubbling is very similar with that from N_2-bubbled testing (Figure S19).All electrode potentials were expressed in reference to the reversible hydrogen electrode (RHE), according to the Nernst equation: $E_{RHE} = E_{exp} + E^{\theta}_{Ag/AgCl} + 0.0592pH$. 5 mg of the catalysts were dispersed in 1.2 mL of 1:1 v/v water/alcohol with 20 μL Nafion by sonication to form a homogeneous suspension. Typically, 10 μL well-dispersed suspension (corresponding to a catalyst loading of 0.209 mg cm^{-2}) was dropped on the glassy carbon electrode and then dried in an ambient environment for measurements. Linear sweep voltammetry (LSV) was tested with a scan rate of 5 mV s^{-1} at 1600 rpm on rotating disc electrode (RDE) with *iR* compensation (correction of the voltage drop caused by resistance), which was done by the method of positive feedback, and the compensation level is 95%. The chronoamperometry (CA) was tested at an overpotential of -0.05V vs RHE after equilibrium. A flow of N_2 was maintained over the electrolyte during the experiment to eliminate dissolved dioxygen.

Calculation details

The density functional theory (DFT) calculations were performed by the Dmol^3 module in Materials Studio 5.5 package, and generalized gradient approximation (GGA) with Perdew-Becke-Ernzerhof (PBE)[2] was used for the exchange-correlation functional. All of the models are calculated in a periodically repeated slab with a dimension of 9.84 Å ×9.84 Å × 15.4 Å to separate the interaction between periodic images. The Game scheme with 2 × 2 × 1 k-point mesh was used to represent the Brillouin zone. The energy, gradient and displacement convergence criterions were set as 1×10^{-5} Ha, 2×10^{-3} Å and 5×10^{-3} Å, respectively. The free energy of the adsorbed state was calculated as

$$\Delta G_{H^*} = \Delta E_{H^*} + \Delta E_{ZPE} - T\Delta S$$

where ΔE_{H^*} is the hydrogen chemisorption energy, and ΔE_{ZPE} is the difference corresponding to the zero point energy between the adsorbed state and the gas phase. As the vibrational entropy of H* in the adsorbed state is small, the entropy of adsorption of 1/2 H_2 is $\Delta S_H \approx -0.5 S_{0H_2}$, where S_{0H_2} is the entropy of H_2 in the gas phase at the standard conditions. Therefore the overall corrections were taken as in[3,4]

$$\Delta G_{H^*} = \Delta E_{H^*} + 0.24 \text{ eV}$$

S2. Supporting Figures and Tables

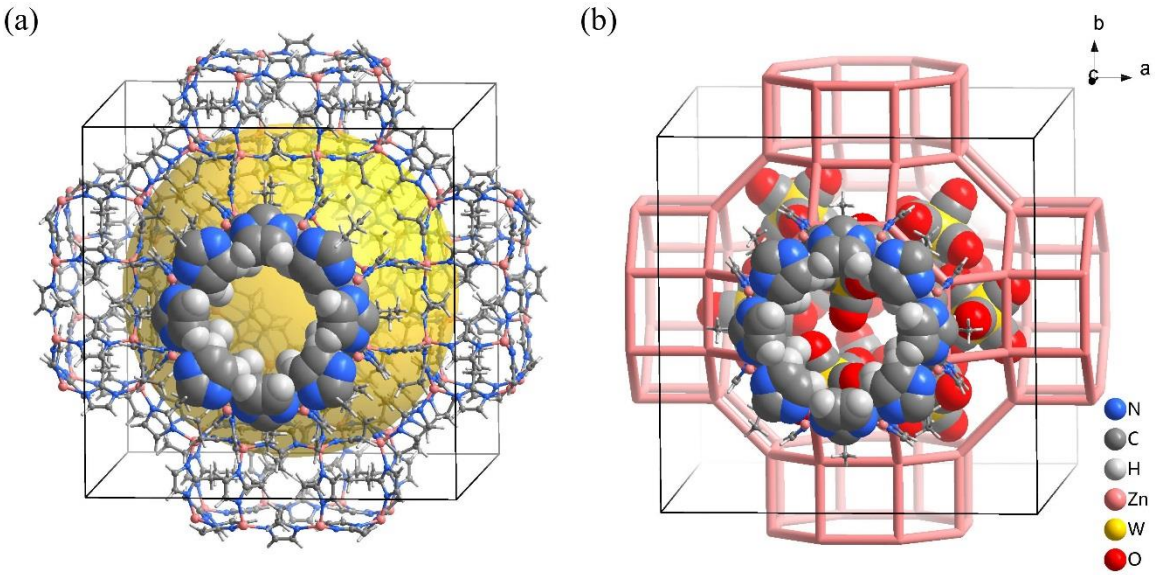

Figure S1. Perspective views of (a) the cage-based coordination framework of MAF-6 and (b) the cage-confined model of $W(CO)_6$@MAF-6 (derived from GCMC simulation).

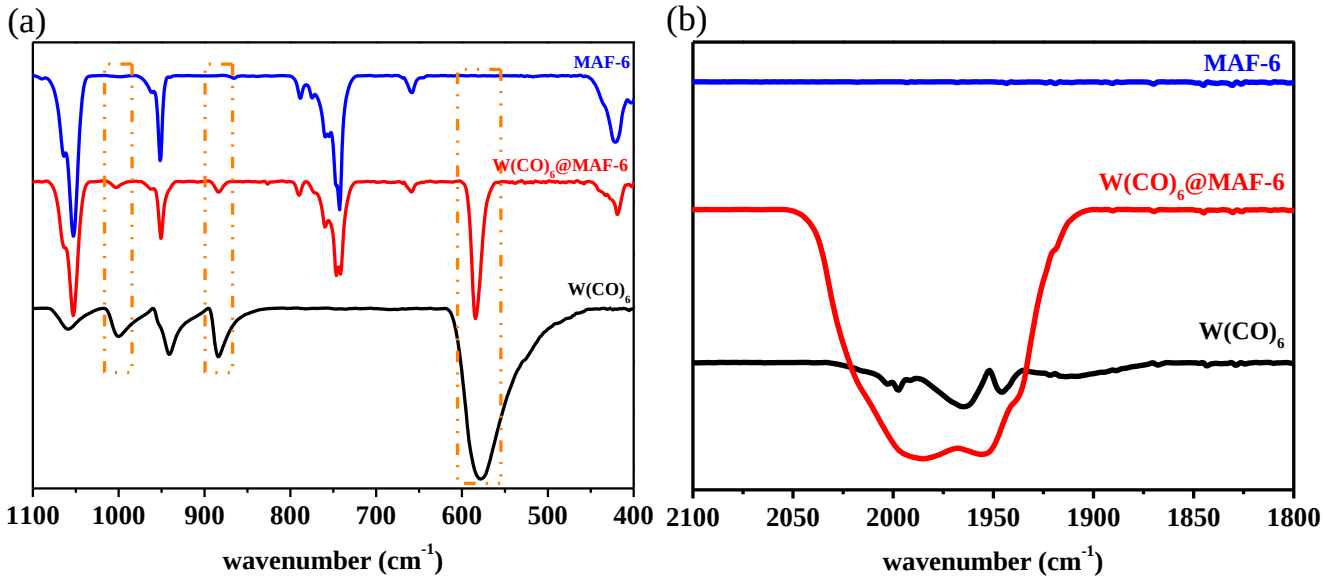

Figure S2. FT-IR spectra of MAF-6, $W(CO)_6$ and $W(CO)_6$@MAF-6 at (a) 400-1100 cm^{-1} and (b) 1800-2100 cm^{-1}.

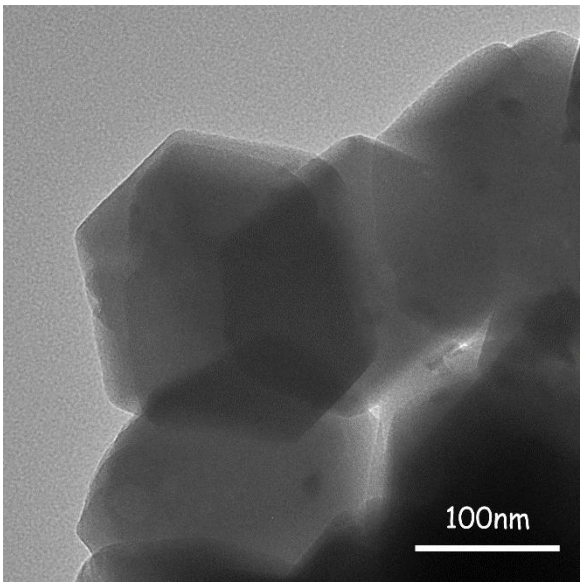

Figure S3. TEM image of $W(CO)_6$@MAF-6.

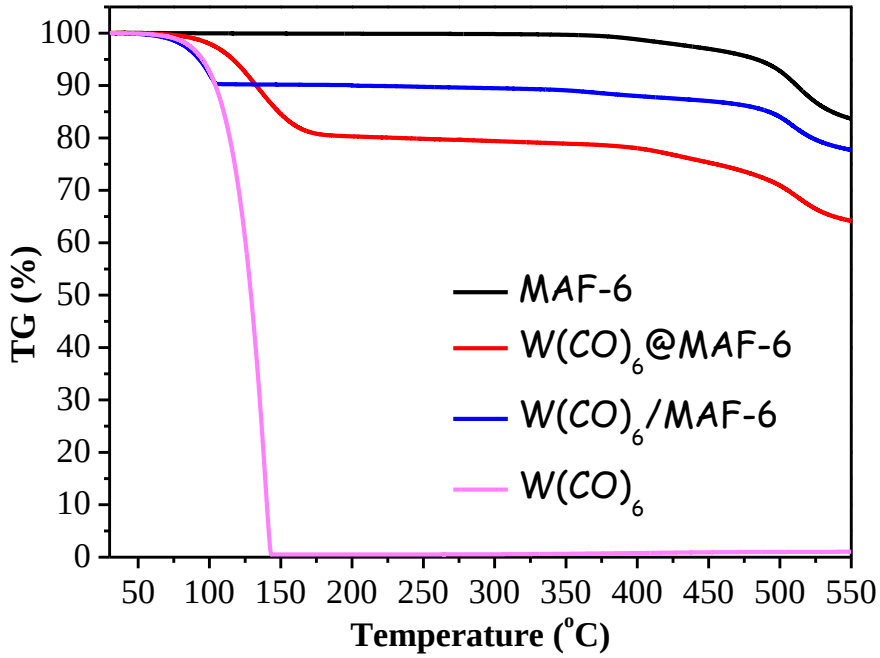

Figure S4. TG curves of $W(CO)_6$, MAF-6, $W(CO)_6$@MAF-6 and $W(CO)_6$/MAF-6.

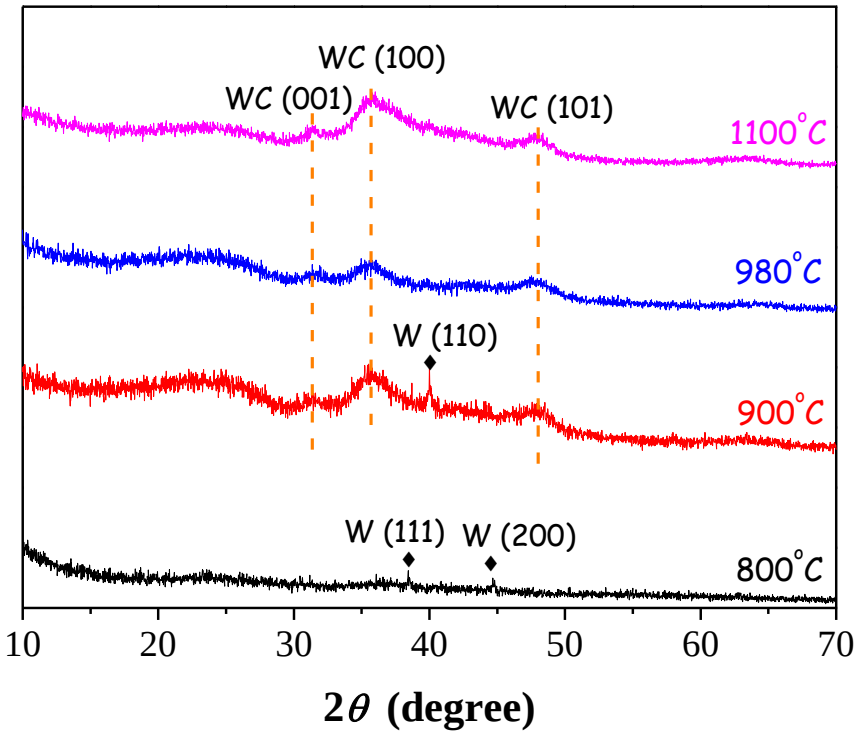

Figure S5. PXRD patterns of samples carbonized at different temperatures.

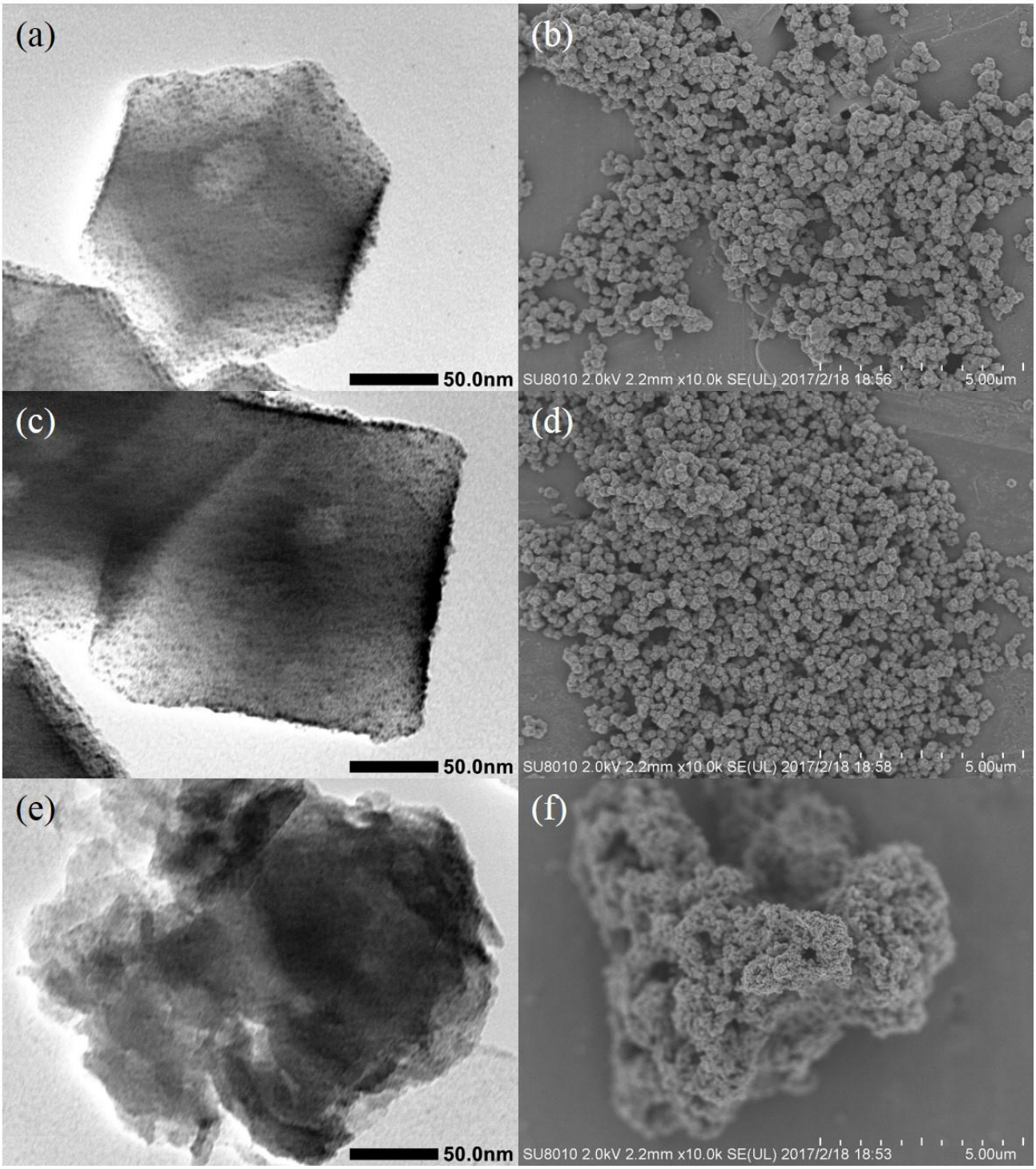

Figure S6. TEM and SEM images of samples carbonized at (a, b) 800 ^{o}C, (c, d) 900 ^{o}C and (e, f) 1100 ^{o}C, respectively.

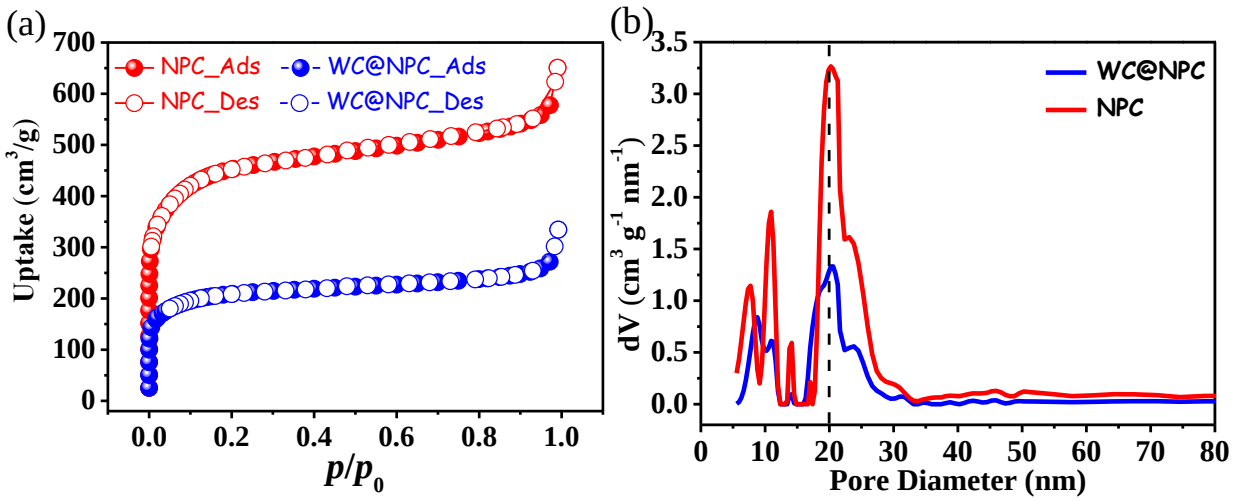

Figure S7. (a) 77 K N_2 adsorption isotherms of WC@NPC and NPC; and (b) their pore size distributions calculated by cylindrical pores model based on DFT.

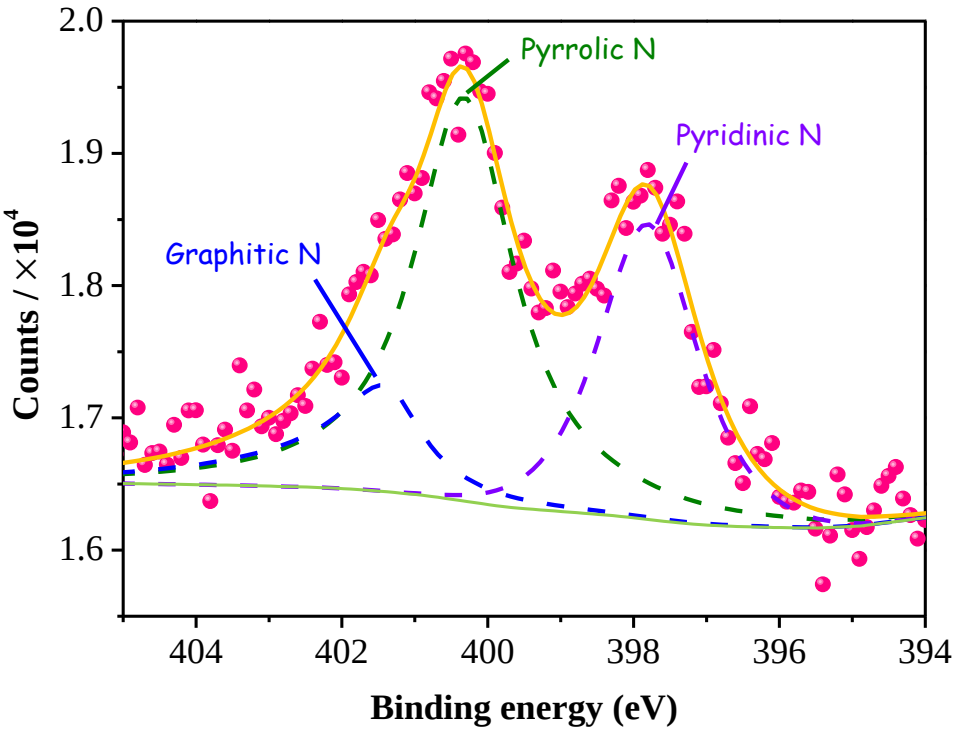

Figure S8. High resolution N1s XPS spectra of WC@NPC.

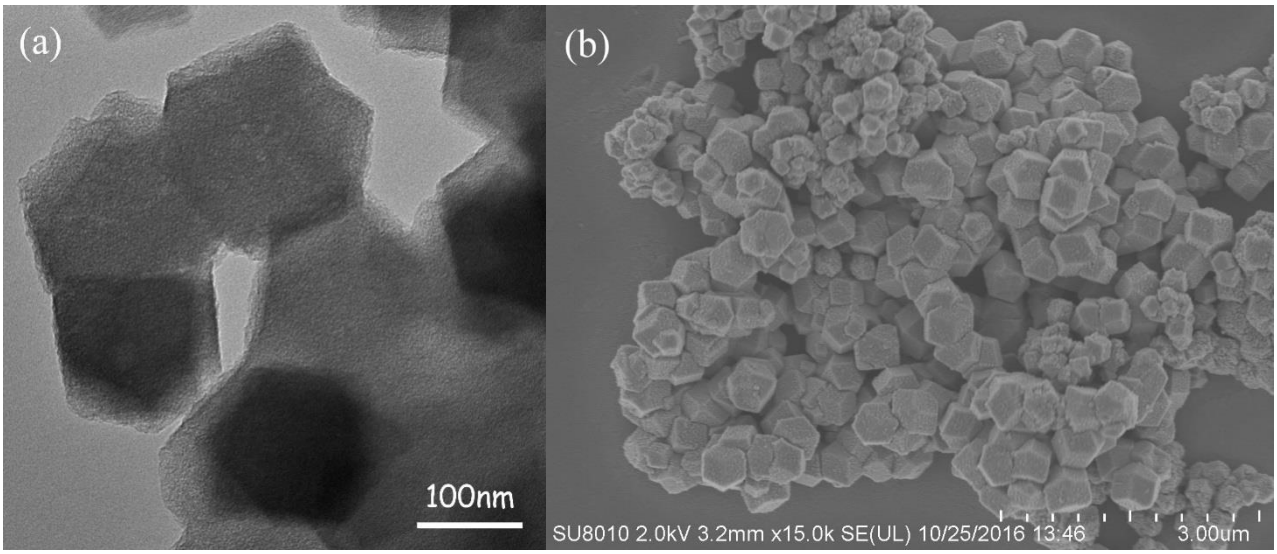

Figure S9. (a) TEM and (b) SEM images of NPC.

Figure S10. SEM image of WC@NPC

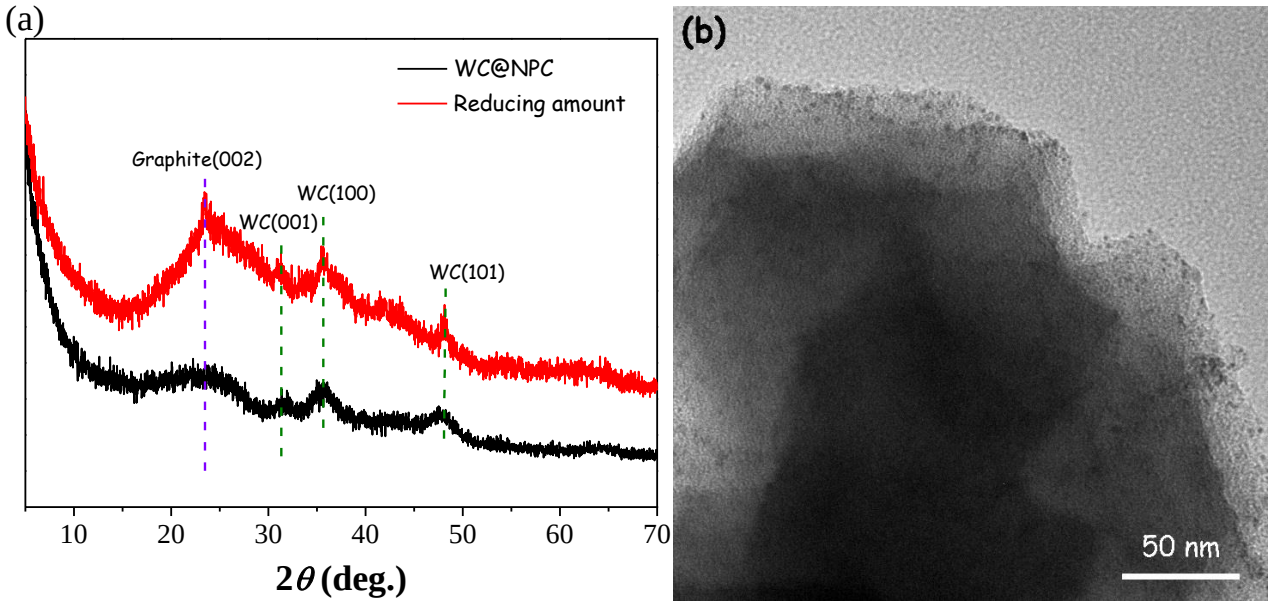

Figure S11. (a) PXRD pattern and (b) TEM image of the sample carbonized by the precursor with lower (9.1 wt%) $W(CO)_6$ loading amount.

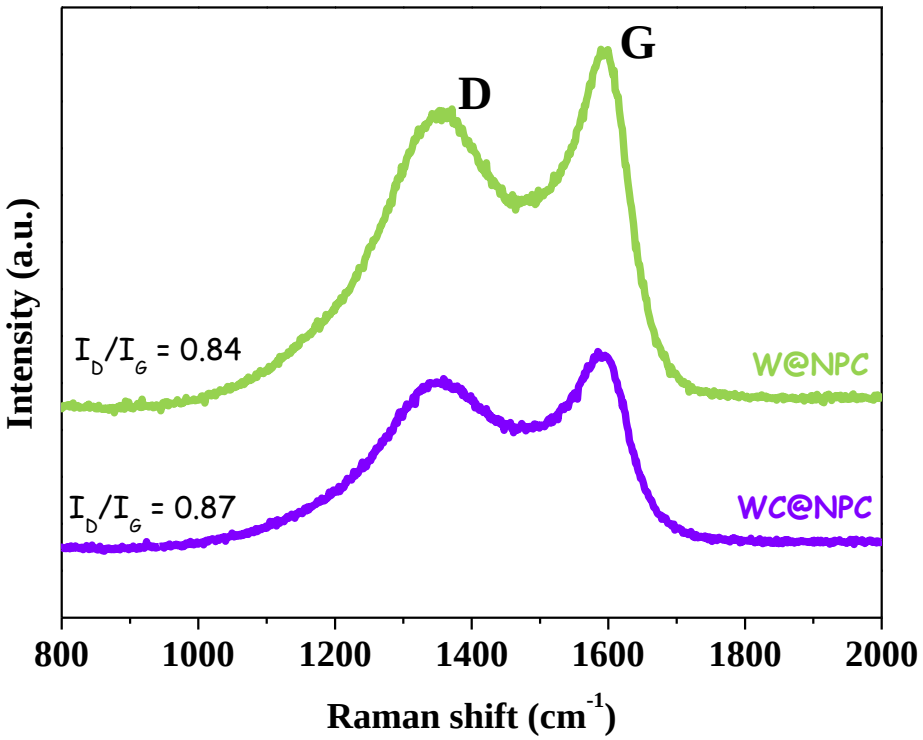

Figure S12. Raman spectra of W@NPC and WC@NPC. There are 2 peaks located at 1350 and 1600 cm^{-1}, corresponding to D (from in-plane imperfections such as defects and heteroatoms of the graphitic lattice of the disordered sp^2-hybridized carbon) and G (from the tangential stretching mode of highly ordered pyrolytic graphite) bands, respectively. The tiny differences between the values of I_D/I_G demonstrate their similar graphitic degree, which indicates that the variety of HER catalytic activity was not led by conductivity differences.

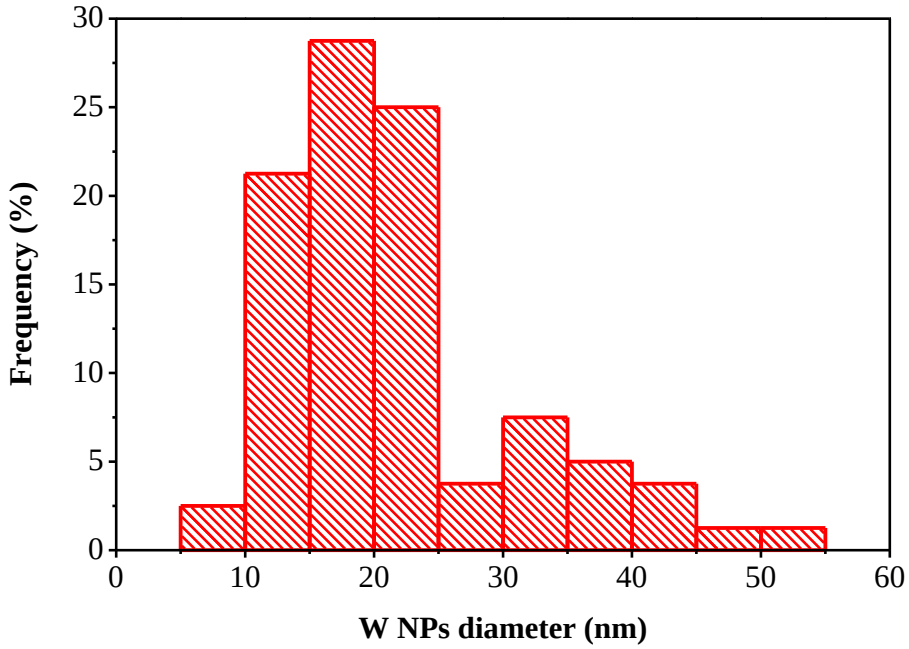

Figure S13. Particle size distribution of W in W@NPC.

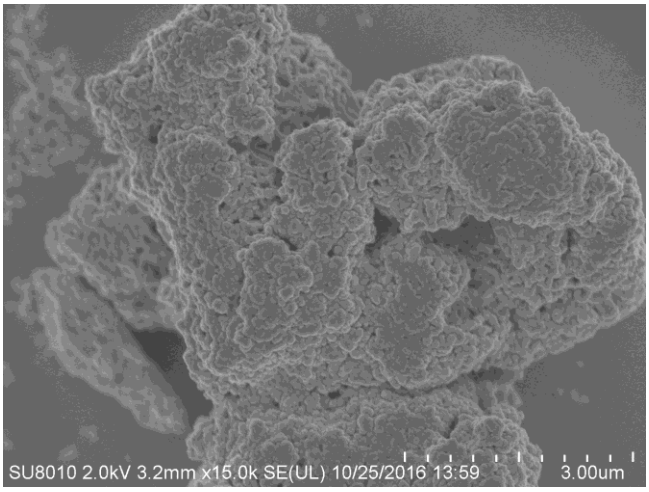

Figure S14. SEM images of W@NPC.

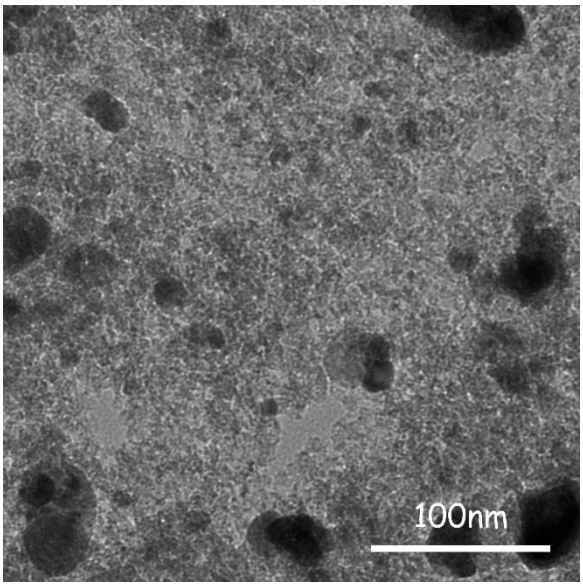

Figure S15. TEM image of W@NPC.

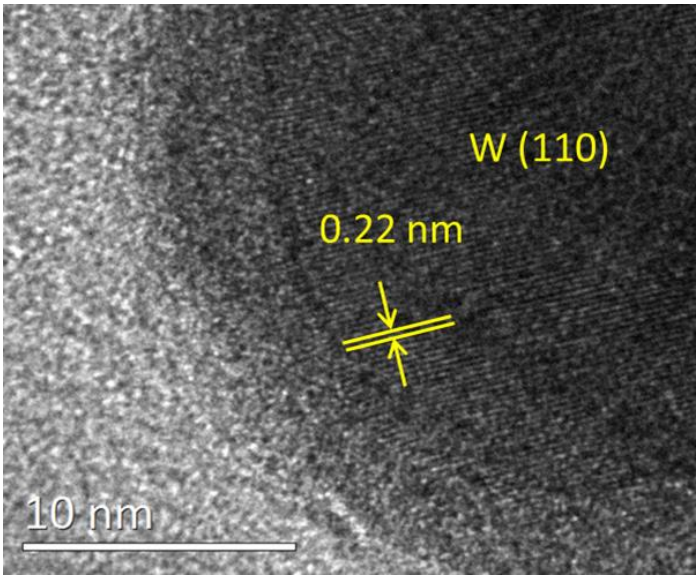

Figure S16. HRTEM image of W@NPC.

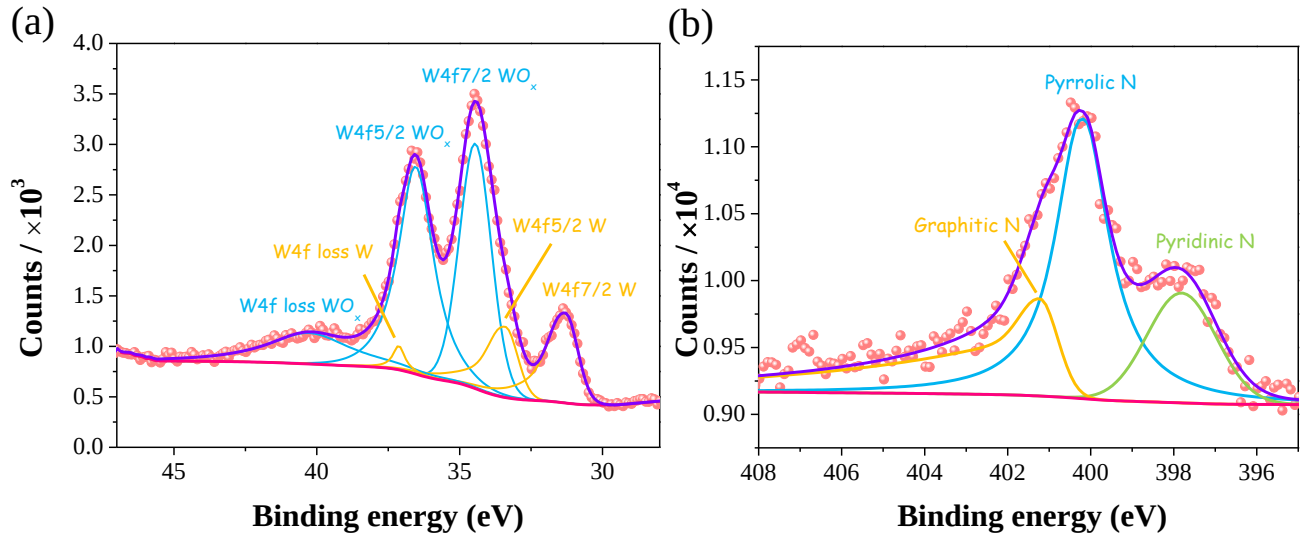

Figure S17. High resolution (a) W4f and (b) N1s XPS spectra of W@NPC.

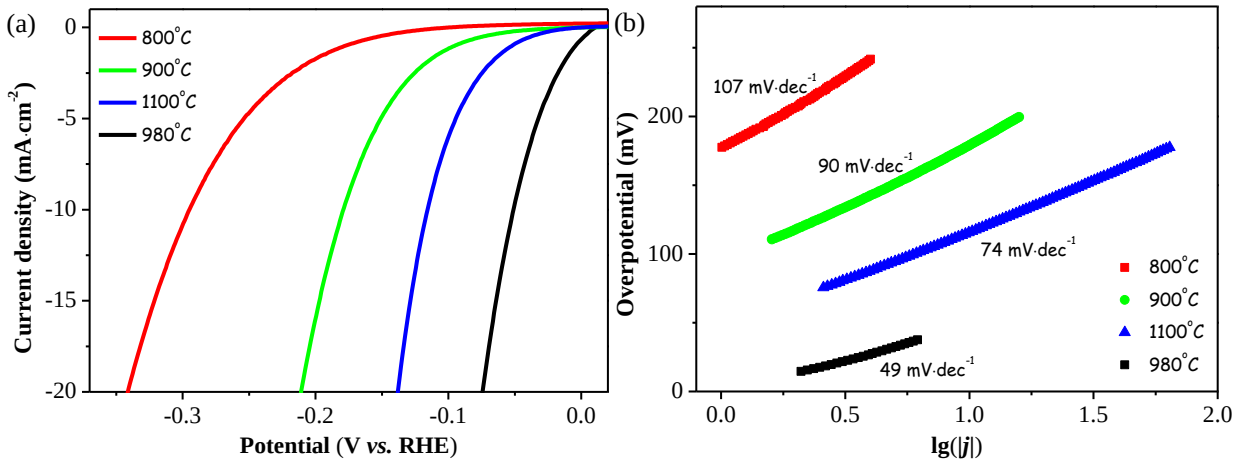

Figure S18. (a) HER polarization and (b) Tafel curves of samples carbonized at different temperatures.

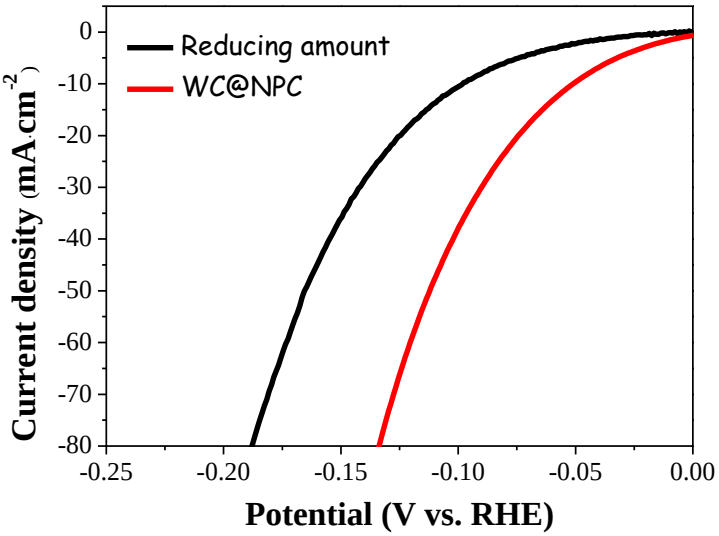

Figure S19. LSV curves of the titled material WC@NPC and that carbonized by reducing loading amount of $W(CO)_6$ from 23 wt% to 9.1 wt%.

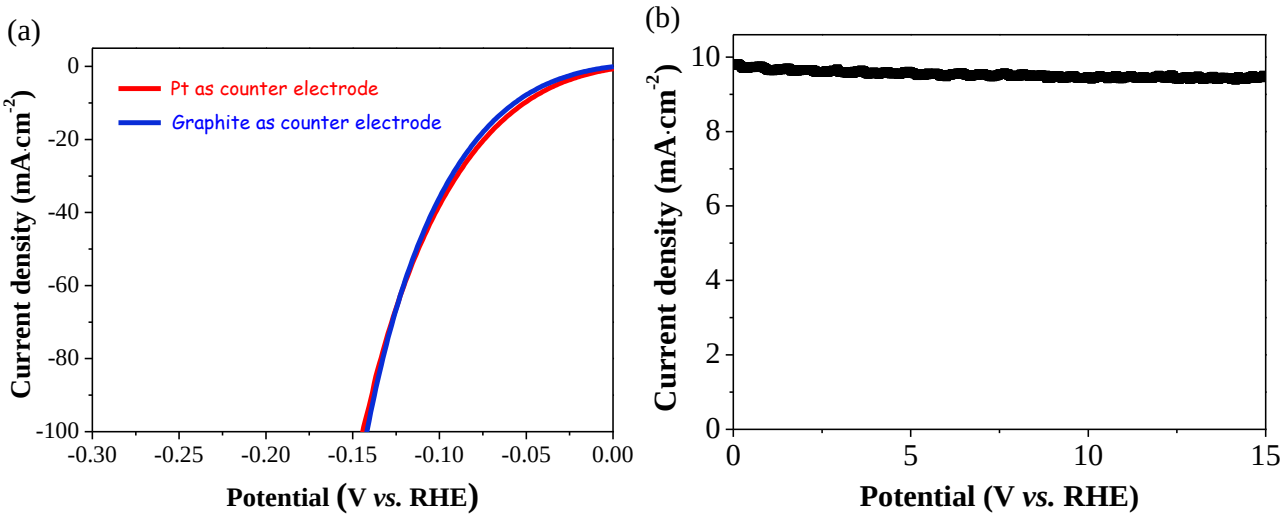

Figure S20. (a) LSV and (b) *i-t* curves of WC@NPC by using graphite as counter electrode.

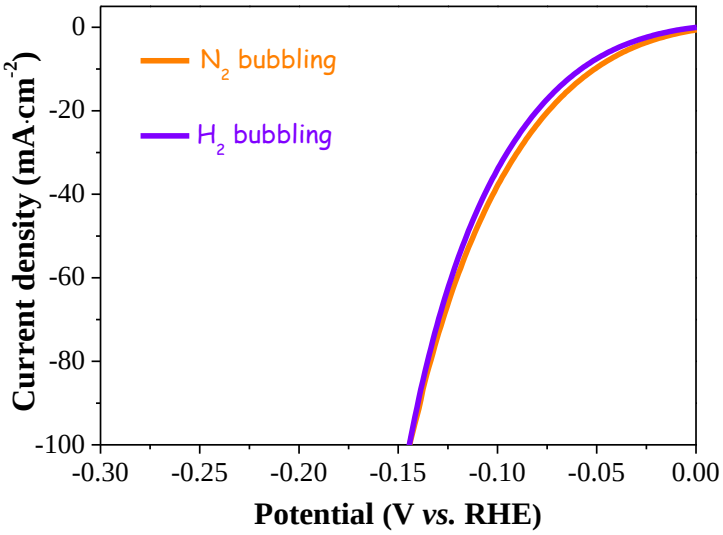

Figure S21. LSV curves of WC@NPC with N_2/H_2 bubbled electrolyte in 0.5 M H_2SO_4.

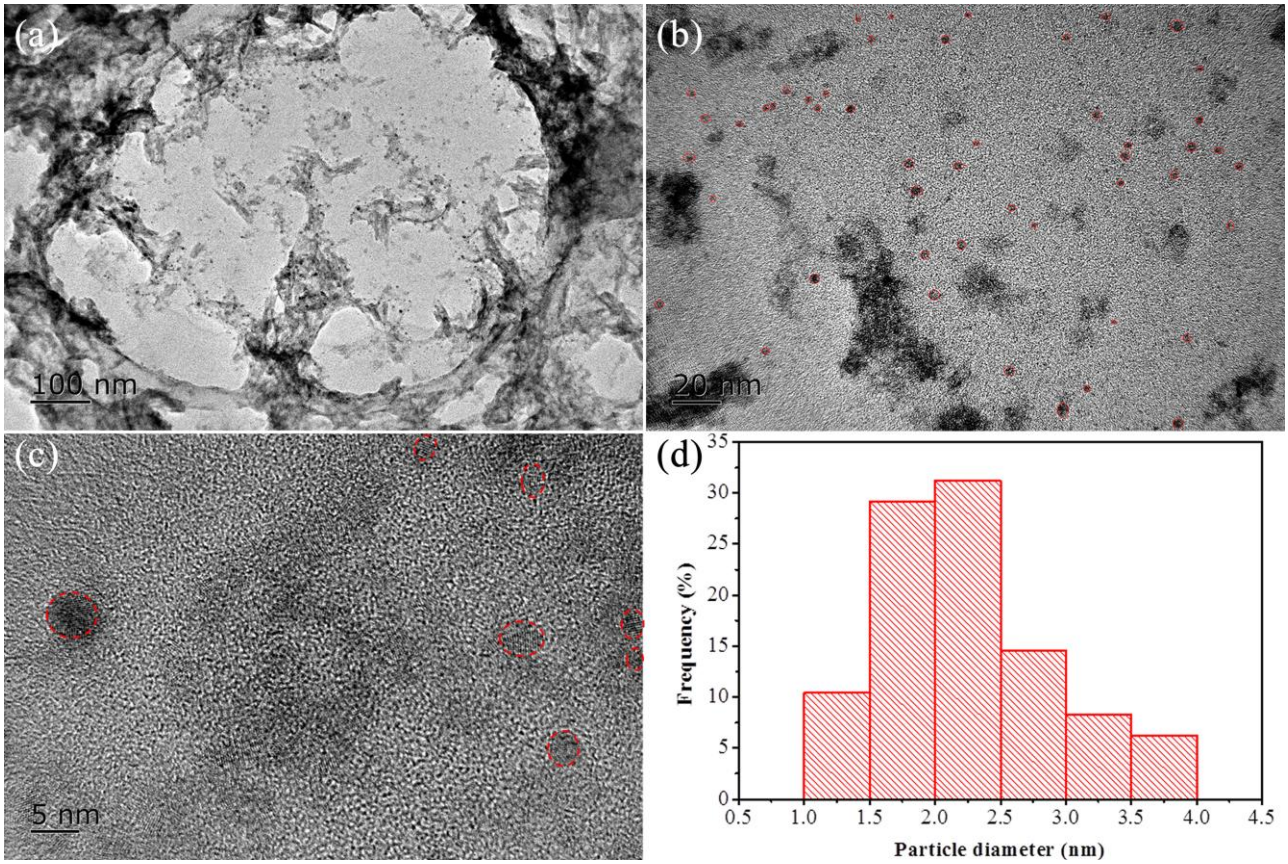

Figure S22. (a, b) TEM, (c) HRTEM images and (d) particle size distribution of WC@NPC after 5-hour HER catalysis.

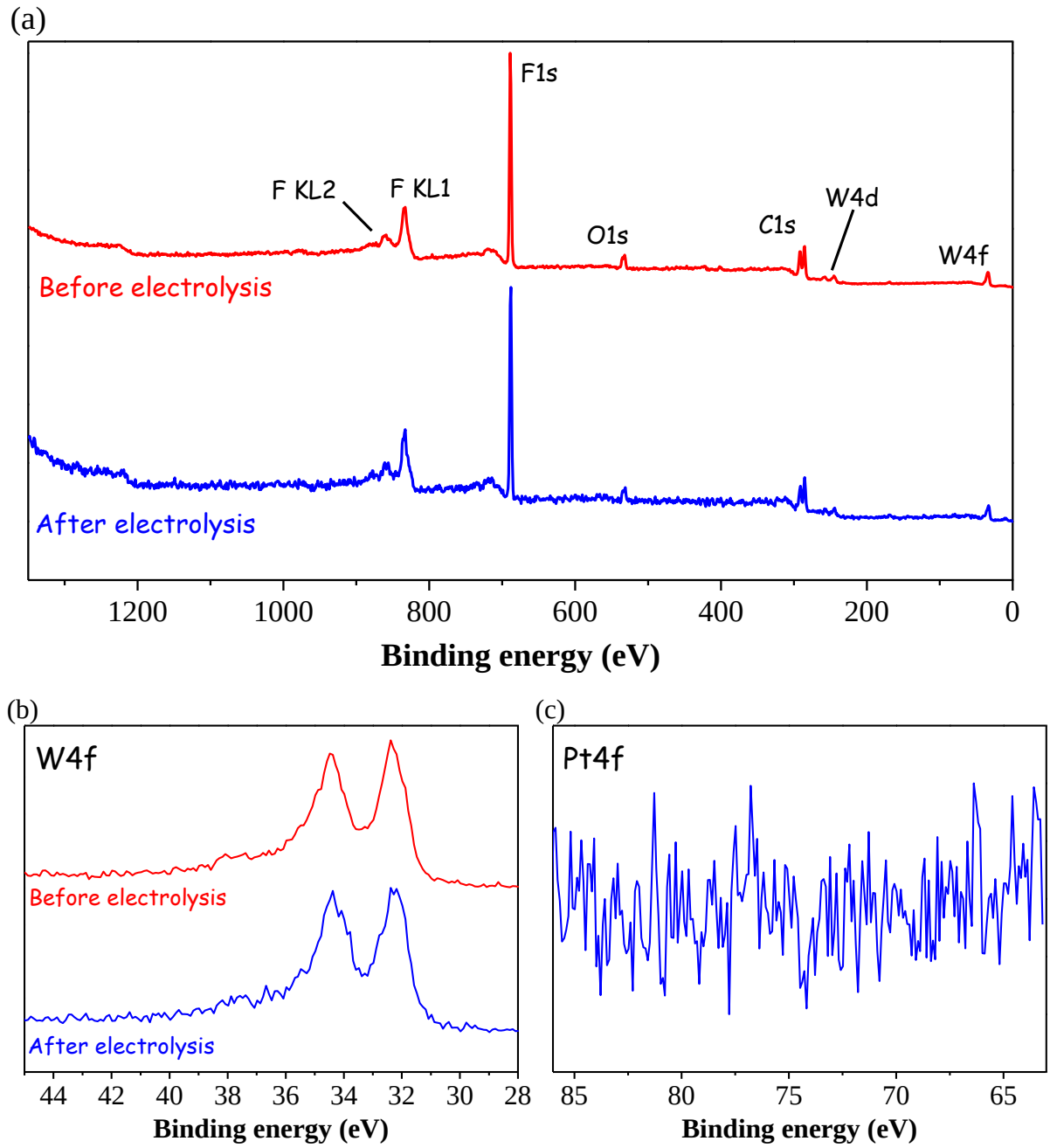

Figure S23. XPS (a) spectra and (b) high-resolution W4f spectra of WC@NPC on the electrode surface before and after HER electrolysis, and (c) high-resolution Pt4f spectrum after electrolysis, which excluded the possibility of Pt deposition during HER. Note: F signals were from Nafion.

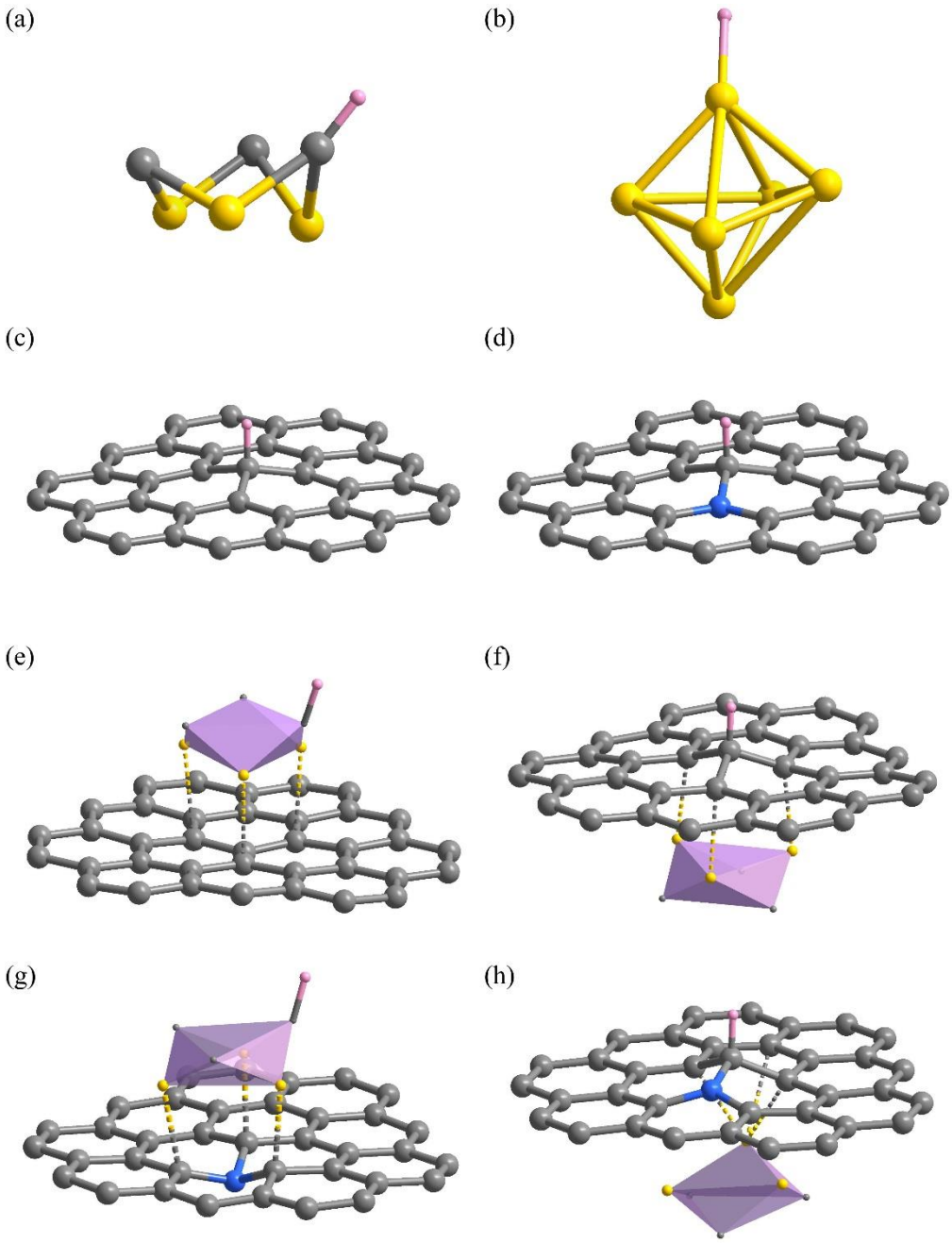

Figure S24. The optimized models of H* adsorption on (a) WC (W_3C_3 cluster), (b) W (W_6 cluster), (c) graphene (Graphene), (d) *N*-doping graphene (*N*-Graphene), (e) the metal side (WC@Gra_WC) and (f) graphene side (WC@Gra_Gra) of WC bonded on graphene (WC@Gra), and (g) the metal side (WC@N-Gra_WC) and (h) graphene side (WC@N-Gra_Gra) of WC bonded on *N*-doping graphene (WC@N-Gra) for DFT calculations. (Gray: C; blue: N; gold: W; pink: H)

Table S1. Comparison of Molybdenum / Tungsten carbides particle sizes and synthesis methods.

Composite	Size / nm	Synthesis method	Ref.
WC@NPC	2	Cage-confinement pyrolysis at 980°C	This work
β-$Mo_{0.06}W_{0.94}C$/CB	most of 1-4	SiO_2-assisted carburization at 900°C	*Angew. Chem. Int. Ed*. **2014**, *53*, 5131
WC	micro-scale	Carburization of LiCl/KCl/KF/W/MWCNT at 950°C	*J. Mater. Chem. A*, **2015**,*3*, 10085
WC	~40nm	Carburization with CH_4/H_2 at 800°C	*Chem. Commun*., **2013**, *49*, 4884
WC	micro-scale	Carburization of WO_3/carbon black at 1300°C	*Chem. Commun*., **2012**, *48*, 1063
PdFe-WC/C	4.1	intermittent microwave heating (IMH) method	*Energy Environ. Sci.*, **2011**, *4*, 558
W_2C/WC/WN mixture	5-20	Carburization of biomass precursors at 850°C	*J. Mater. Chem. A*, **2015**, *3*,18572
WC	3-6	"Urea Glass" Route (Carburization at 800°C)	*Nano Lett.*, **2008**, *8*, 4659
WC	~21.6	hot filament chemical vapor deposition (HF-CVD) at 1050°C	*ACS Nano*, **2015**, *9*, 5125
β-$Ta_{0.3}W_{0.7}C$/CB	most of 2-3	SiO_2-assisted carburization at 900°C	*J. Phys. Chem. C*, **2015**, *119*, 13691
WC/W_2C mixture	5-25	Carburization of W-orthoester precursor with mpg-C_3N_4 above 800°C	*ChemSusChem*, **2013**, *6*, 168
Pt–WC_{THP}/G	3-9	Microwave assisted synthesis	*Nano Energy*, **2014**, *8*, 52
WC/CNT	200	Carburization of $(NH_4)_6H_2W_{12}O_{40}$/CNT with CH_4/H_2 at 900°C	*Electrochim. Acta*, **2007**, *52*, 2018
WC_{1-x}/Pt/MWNT	7.5	Sonochemical method and carburization at 450°C	*J. Power Sources*, **2009**, *193*, 441

WC/W_2C mixture	1.9±0.9	Modified arc-discharge method at CH_4atmosphere	*Nano Energy*, **2016**, *28*, 261
Pt/TiWC	3	SiO_2-assisted carburization at 900°C	*Science*, 2016, 352, 974
W_2C/WN mixture	11/2.9	Carburization of ammonium tungstate/graphene/aniline at 900°C	*ChemSusChem* **2014**, *7*, 2414
Co_6W_6C	5-20	Carburization of dicyandiamide/$Co(NO_3)_2$/$(NH_4)_2WO_4$ at 700°C	*Nanoscale*, **2015**, *7*, 3130
Fe-WC/WN mixture	10-20	Carburization of polydiaminopyridine/H_2WO_4/$Fe(NO_3)_3$ at 700°C	*Angew. Chem. Int. Ed*. **2013**, *52*, 13638
WC	20	High-energy ball milling	*Inorg. Mater.*, **2009**, *45*, 380
W_2C	most of 2-5	Carburization at 800°C with low pressure 320 Pa	*Nat.Commun.*, **2016**, *7*, 16216
β-Mo_2C/η-MoC mixture	8	Carburization of POM-MOF at 800°C	*Chem. Mater.* **2016**, *28*, 6313
N, *P*-doped Mo_2C@C	8.5	Carburization of phosphomolybdic acid/polypyrrole at 800°C	*ACS Nano* **2016**, *10*, 8851
Mo_2C	5-20	Carburization of $(NH_4)_6Mo_7O_{24}\cdot 4H_2O$/dicyandiamide at 800°C	*ACS Nano* **2016**, *10*, 10397
Mo_2C/MoO_2/MoO_3/MoN mixture	1-3	Carburization of $(NH_4)_6Mo_7O_{24}\cdot 4H_2O$/dicyandiamide with 2-step heating (400 and 800°C)	*Angew. Chem. Int. Ed.* **2015**, *54*, 14723
Mo_2C/CNT	7-15	Carburization of carbon-supported $(NH_4)_6Mo_7O_{24}\cdot 4H_2O$ at 800°C	*Energy Environ. Sci.*, **2013**, *6*, 943
MoS_2/Mo_2C-NCNTs mixture	135	Carburization MoO_3/PANI at 700°C	*J. Mater. Chem. A*, **2014**, *2*, 18715
MoC_x/C	5-50	Carburization of polyoxometalate-encapsulated	*J. Mater. Chem. A*,

		coordination polymer at 800°C	**2016**, *4*, 3947
$Mo_2C/MoN/MoO_3$ mixture	20-30	CO_2emission assisted pyrolyzed at 800 °C	*J. Am. Chem. Soc.* **2015**, *137*, 110
Mo_2C	11	Urea glass route	*J. Mater. Chem. A*, **2015**, *3*, 8361
η-MoC/ η-MoC_{1-x} mixture	4-10	Carburization of MOF (NENU-5) at 800°C	*Nat. Commun.*, **2015**, *6*, 6512;
β-Mo_2C/γ-Mo_2N mixture	10-20	Carburization of biomass precursors at 800°C	*Energy Environ. Sci.*, **2013**, *6*, 1818
Mo_2C/NCF	3	Self-polymerization of dopamine with $(NH_4)_6Mo_7O_{24}\cdot 4H_2O$ and carburization at 750°C	*ACS Nano*, **2016**, 10, 11337

Table S2. Analytcial results of elemental containing by EDS.

	C wt%	N wt%	O wt%	W wt%	Zn wt%
WC@NPC	41.8	3.5	6.7	48.0	0
W@NPC	48.8	2.0	7.5	41.7	0
800°C carbonization	30.5	5.2	7.8	48.2	8.3
900°C carbonization	41.3	2.5	5.6	45.7	4.8
1100°C carbonization	39.4	3.0	6.1	51.5	0
carbonized with less $W(CO)_6$ loading	57.7	4.4	8.1	29.8	0

Table S3. Comparison of HER catalytic performances of reported Mo/W-containing catalysts in 0.5 M H_2SO_4 solution.

Catalyst	Loading (mg cm^{-2})	η_{10} (mV *vs* RHE)	E_{onset} (mV *vs* RHE)	Tafel slop (mV dec^{-1})	j_0 (mA cm^{-2})	Reference
WC@NPC	0.209	51	0	49	2.4	This work
W@NPC	0.209	233 (@2 mA cm^{-2})	28	191	1×10^{-4}	This work
20% Pt/C	0.209	30	0	22	1.2	This work
β-$Mo_{0.06}W_{0.94}C$/CB	0.704	220	N/A	N/A	N/A	*Angew. Chem. Int. Ed.*, **2014**, *53*, 5131
α-WC/CB	0.704	256	N/A	N/A	N/A	
$WSoy_{0.7}GP_{1.0}$ (WC/W_2C/WN/Graphene)	2.2	105	N/A	36	0.063	*J. Mater. Chem. A*, **2015**, *3*, 18572
porous WC film	0.16	275	120	69	N/A	*J. Mater. Chem. A*, **2015**, *3*, 5798
porous WS_2 film	0.08	265	100	67	N/A	
WC-1050	N/A	145	15	72	N/A	*ACS Nano*, **2015**, *9*, 5125
β-$Ta_{0.3}W_{0.7}C$/CB	0.704	242	100	72	N/A	*J. Phys. Chem. C*, **2015**, *119*, 13691
Fe-WCN	0.4	220	N/A	47	N/A	*Angew. Chem. Int. Ed.*, **2013**, *52*, 13638
C-CWC	0.28	200	26	75	0.0286	*Nanoscale*, **2015**, *7*, 3130
MoS_2/WC/RGO	0.104	202	110	41	N/A	*Chem. Commun.*, **2013**, *49*, 4884
W_2C-1073	1	190	130	102	0.28	*ChemSusChem*, **2013**, *6*, 168
WC-1223	1	150	190	84	0.35	
W_2C/GnP	2.2	186	N/A	64.7	0.024	*ChemSusChem*, **2014**, *7*, 2414
$W_{0.5}$Ani/GnP	0.96	120	N/A	68.6	0.038	

W_2C/MWNT	0.56	123	50	45	N/A	*Nat. Commun.*, **2016**, *7*, 13216
P-WN/rGO	0.337	85	46	54	0.35	*Angew. Chem. Int. Ed.*, **2015**, *54*, 6325
WP_2 SMPs	0.5	161	54	57	0.017	*ACS Catal.*, **2015**, *5*, 145
WSe_2 nanofilm	N/A	300	N/A	77.4	N/A	*Nano Lett.*, **2013**, *13*, 3426
WS_2@P,N, O-graphene	0.113	125	N/A	52.7	0.131	*Adv. Mater.*, **2015**, 27, 4234
MWCMNs(WO_2)	0.35	58	35	46	0.64	*J. Am. Chem. Soc.*, **2015**, *137*, 6983
$W_{18}O_{49}$@WS_2 NRs	0.3	310	170	86	N/A	*Chem. Commun.*, **2015**, *51*, 8334
W-CNT	N/A	435	N/A	103	N/A	*J. Mater. Chem. A*, **2015**, *3*, 14609
WS_2 nanosheet	1	142	75	70	N/A	*Energy Environ. Sci.*, **2014**, *7*, 2608
WS_2@rGO	0.4	270	N/A	58	N/A	*Angew. Chem. Int. Ed.*, **2013**, *52*, 13751
nw-W_4Mo	1.28	128	N/A	52	0.029	*Adv. Funct. Mater.*, **2015**, *25*, 1520
WS_2	0.43	152	80	46	N/A	*Nanoscale*, **2016**, *8*, 15262
a-WNP (W-Ni_xP)	1	110 (@ 20 mA cm^{-2})	50	39	0.044	*J. Mater. Chem. A*, **2014**, *2*, 18593
WSe_2-C-20	N/A	158	N/A	98	0.24	*J. Mater. Chem. A*, **2015**, *3*, 18090
$Co_xW_{(1-x)}S_2$	N/A	121	N/A	67	N/A	*Small*, **2016**, *12*, 3802

Co_9S_8@MoS_2/CNFs	0.212	190	64	110	N/A	*Adv. Mater.*, **2015**, *27*, 4752
NiMoN	2.5	109	50	95	0.92	*Adv. Energy Mater.*, **2016**, *6*, 1600221
$NiMo_3S_4$ hollow plates	0.3	257	59	98	0.039	*Angew. Chem. Int. Ed.*, **2016**, *55*, 15240
Co-Mo_2C-0.02	0.14	140	40	39	5.1×10^{-3}	*Adv. Funct. Mater.*, **2016**, *26*, 5590
SV-MoS_2	N/A	170	N/A	60	N/A	*Nat. Mater.*, **2016**, *15*, 48
NENU-500 (Mo-MOF)	0.362	237	180	96	0.036	*J. Am. Chem. Soc.*, **2015**, *137*, 7169
nanoMoC@GS(700)	1.04	124	N/A	43	0.015	*J. Mater. Chem. A*, **2016**, *4*, 6006
Co-Mo-S hierarchical nanosheets	N/A	203 (@100 mA cm^{-2})	90	53	N/A	*J. Mater. Chem. A*, **2016**, *4*, 13731
Amorphous MoP NP	1	90	N/A	45	0.12	*Chem. Mater.*, **2014**, *26*, 4826
MoP@PC	0.24	51	N/A	45	N/A	*Adv. Funct. Mater.*, **2015**, *25*, 3899
$Co_{0.6}Mo_{1.4}N_2$	0.243	200	N/A	N/A	0.23	*J. Am. Chem. Soc.*, **2013**, 135, 19186
PDAP-MoCN-CO_2	0.4	140	50	46	N/A	*J. Am. Chem. Soc.*, **2015**, *137*, 110
MoS_2@S-C_{PDA}	N/A	160	60	72	0.316	*Chem. Commun.*, **2015**, *51*, 5052
Mo-W-P/CC	N/A	138 (@ 100 mA cm^{-2})	N/A	31	0.288	*Energy Environ. Sci.*, **2016**, *9*, 1468

MoO_2P_x/Mo foil	0.1	135	80	62	N/A	*J. Mater. Chem. A*, **2016**, *4*, 1647
MoC_x@C-1	0.354	79	N/A	56	0.27	*J. Mater. Chem. A*, **2016**, *4*, 3947
MoP_2 NP/Mo plate	N/A	143	N/A	57	0.06	*Nanoscale*, **2016**, *8*, 8500
MCNS/NC (Mo_2C nanosheet)	0.566	19	0	28.9	1.9	*Nanoscale*, **2016**, *8*, 16251
Mo_2C@C S-800	0.9	141	N/A	56	0.029	*ACS Nano*, **2016**, *10*, 8851
NiMo-NGTs	2	65	N/A	67	0.84	*ACS Nano*, **2016**, *10*, 10397
Mo_2C/CNT	2	152	N/A	55.2	0.014	*Energy Environ. Sci.*, **2013**, *6*, 943
MoS_2 on graphene	N/A	100	70	41	0.0182	*Chem. Mater.*, **2016**, *28*, 549
$MoSe_2$-NiSe	0.285	210	150	74	N/A	*Chem. Mater.*, **2016**, *28*, 1838
HC800 (Ni-Mo_2C)	0.12	192	N/A	98	N/A	*Chem. Mater.*, **2016**, *28*, 6313
4L-MoS_2	0.3	178	120	60	N/A	*ACS Nano*, **2015**, *9*, 3728
MoP@PC	0.41	153	77	66	0.21	*Angew. Chem. Int. Ed.*, **2016**, *55*, 12854
β-Mo_2C nanotube	0.75	172	82	62	0.017	*Angew. Chem. Int. Ed.*, **2015**, *127*, 15615
MoC_x	0.8	142	25	53	0.023	*Nat. Commun.*, **2015**, *6*, 6512;
MoP@PC	0.41	153	77	66	0.21	*Angew. Chem. Int. Ed.*, **2016**, *55*, 12854
MoO_2@PC-rGO	0.14	64	0	41	0.48	*Angew. Chem. Int. Ed.*,

						2015, *54*, 12928
Mo_1Soy/rGO	0.47	109	N/A	62.7	0.037	*Energy Environ. Sci.*, **2013**, *6*, 1818
C-MoS_2	N/A	159	103	56.1	N/A	*Nano Energy*, **2016**, *22*, 490
Li-MoS_2 NS/CC	4	97	75	38	N/A	*Carbon*, **2016**, *98*, 84
MoS_2/g-C_3N_4	0.3	140	26	45	8×10^{-3}	*Nano Energy*, **2016**, *27*, 44
CM-S ($Cu_2MoS_ySe_{4-y}$)	2	170	96	52	N/A	*Nano Energy*, **2016**, *28*, 366
np-Mo_2C NWs	0.21	130	70	60	N/A	*Energy Environ. Sci.*, **2014**, *7*, 387
Mo_2C	0.102	198	N/A	56	N/A	*J. Mater. Chem. A*, **2015**, *3*, 8361
MoDCA-5	0.25	78	6	41	0.179	*Angew. Chem. Int. Ed.*, **2015**, *54*, 14723
Mo_2C@NPC/NPRGO	0.14	34	0	33.6	1.09	*Nat. Commun.*, **2016,** *7*, 11204
$MoSe_2$ nanofilm	N/A	250	N/A	59.8	3.8×10^{-4}	*Nano Lett.*, **2013**, *13*, 3426
MoS_2/RGO	0.28	140	100	41	N/A	*J. Am. Chem. Soc.*, **2011**, *133*, 7296
Mo_2C/NCF	0.28	144	40	55	N/A	*ACS Nano*, **2016**, *10*, 11337

*η_{10}: Unless stated, overpotential at 10 mA cm^{-2} current density.

S3. References

(1) He, C.-T.; Jiang, L.; Ye, Z.-M.; Krishna, R.; Zhong, Z.-S.; Liao, P.-Q.; Xu, J.; Ouyang, G.; Zhang, J.-P.; Chen, X.-M. *J. Am. Chem. Soc.* **2015**, *137*, 7217.

(2) Perdew, J. P.; Ernzerhof, M.; Burke, K. *J. Chem. Phy.* **1996**, *105*, 9982.

(3) Nørskov, J. K.; Bligaard, T.; Logadottir, A.; Kitchin, J. R.; Chen, J. G.; Pandelov, S.; Stimming, U. *J. Electrochem. Soc.* **2005**, *152*, J23.

(4) Zheng, Y.; Jiao, Y.; Zhu, Y.; Li, L. H.; Han, Y.; Chen, Y.; Du, A.; Jaroniec, M.; Qiao, S. Z. *Nat. Commun.* **2014**, *5*, 3783.